*Inorg. Chem.* **2009**, *48*, 1826−1835

# Tetra-, Tri-, and Mononuclear Manganese(II/III) Complexes of a Phenol-Based $N_2O_2$ Capping Ligand: Use of Carboxylates as Ancillary Ligands in Tuning the Nuclearity of the Complexes

**Debdas Mandal,[†] Pabitra Baran Chatterjee,[†] Shubhajit Bhattacharya,[†] Ki-Young Choi,[‡] Rodolphe Clérac,[§,||] and Muktimoy Chaudhury*,[†]**

*Department of Inorganic Chemistry, Indian Association for the Cultivation of Science, Kolkata 700 032, India, Department of Chemistry Education, Kongju National University, Kongju 314-701, Republic of Korea, CNRS, UPR 8641, Centre de Recherche Paul Pascal (CRPP), Equipe "Matériaux Moléculaires Magnétiques", 115 avenue du Dr. Albert Schweitzer, Pessac, F-33600, France, and Université de Bordeaux, UPR 8641, Pessac, F-33600, France*

Received June 18, 2008

Manganese(II/III) complexes of a phenol-based tetradentate ligand $L^{2-}$ [$H_2L$ = *N,N′*-dimethyl-*N,N′*-bis(2-hydroxy-3,5-dimethylbenzyl)-ethylenediamine], namely, $[Mn_4(L)_2(PhCOO)_6]$ (**1**), $[Mn_3(L)_2(CH_3CH_2COO)_2(OMe)_2]\cdot H_2O$ (**2**), and $[Mn(L)\{(CH_3)_3CCOO\}(CH_3OH)]\cdot CH_3OH$ (**3**), have been synthesized. The basicity and steric congestion provided by the carboxylate moiety used as an ancillary ligand have profound influence on tuning the nuclearity of these compounds. Results of X-ray crystallography, electronic spectroscopy, and variable-temperature (1.8−300 K) magnetic measurements have been used to characterize these compounds. Complex **1** has a very interesting centrosymmetric structure that involves two crystallographically equivalent binuclear [$Mn^{II}$−$Mn^{III}$] units, connected together by a pair of syn−anti bridging benzoates to generate a "dimer of dimers" structural motif. Compound **2** with propionate as the ancillary ligand, on the other hand, has a nearly linear $Mn^{III}$−$Mn^{II}$−$Mn^{III}$ core with antiferromagnetically coupled ($J = -0.13$ cm$^{-1}$) metal centers. Compound **1** has an $S_T = 9$ spin ground state with ferromagneticly coupled metal centers ($J_{wb}$= 2.8(1) and $J_{bb} = 0.09(2)$ cm$^{-1}$) that failed to function as a single molecule magnet due to the presence of low-lying excited states with smaller spin values and a weak magnetic anisotropy. The electron paramagnetic resonance spectrum of **1** in the frozen solution (12 K) displays two signals in the $g = 2$ and $g = 4$ regions, each split into six lines due to $^{55}$Mn ($I = 5/2$) superhyperfine couplings. The use of bulky pivalate as a replacement for benzoate provides enough steric bulk to generate a mononuclear species $[Mn(L)\{(CH_3)_3CCOO\}(CH_3OH)]\cdot CH_3OH$ (**3**). The lone manganese(III) center in this compound has an octahedral geometry, completed by the tetradentate ligand $L^{2-}$ together with an axially coordinated methanol molecule and a monodentate pivalate. The latter two are connected by a hydrogen bond, thus stabilizing the monodentate carboxylate moiety. Redox behaviors (CV) of **1** and **3** are grossly similar, each undergoing a quasi-reversible reduction process at $E_{1/2} = -0.03$ and $-0.11$ V, respectively, versus a Ag/AgCl reference.

## Introduction

The chemistry of polynuclear manganese with mixed-oxidation states (II−IV) is an area of contemporary research interest.[1−3] The primary reason for such interest stems from the recognition of a tetramanganese complex as the water oxidizing center in a multi-subunit enzyme, photosystem-II (PS-II). PS-II catalyzes the light-driven four-electron oxidation of water into molecular oxygen performed by green plants and cyanobacteria.[1,2] Previously, on the basis of extended X-ray absorption fine structure data, Klein et al.

* To whom correspondence should be addressed. E-mail: icmc@iacs.res.in.
[†] Indian Association for the Cultivation of Science.
[‡] Kongju National University.
[§] Centre de Recherche Paul Pascal.
[||] Université de Bordeaux.

(1) Photosynthetic water oxidation, Special Dedicated Issue: Nugent, J. *Biochim. Biophys. Acta* **2001**, *1503*, 1.
(2) Mukhopadhyay, S.; Mandal, S. K.; Bhaduri, S.; Armstrong, W. H. *Chem. Rev.* **2004**, *104*, 3981.



10.1021/ic801132r CCC: $40.75 
Published on Web 02/03/2009

proposed a "dimer-of-dimers" model for the structure of this tetramanganese cofactor involving two dimanganese units, connected together via a $\mu$-oxo bridge.[4,5] Subsequent information gathered from X-ray structural[6−8] and electron paramagnetic resonance (EPR)/electron nuclear double resonance studies[9,10] suggested an alternative "3 + 1" model for the PS-II cofactor involving a trinuclear manganese core, connected to a fourth metal center.

Syntheses of multinuclear manganese compounds of biomimetic ligands with preorganized donor atoms set can provide valuable information in gaining structural and mechanistic insights into the PS-II active site.[2] Various tetra-[11−22] and trinuclear[23−30] mixed-valence manganese compounds in higher oxidation states have been reported recently as biomimetic models for this active site. Many of these compounds are found to be quite effective in rendering a backup support to the results of X-ray crystallography, collected only at lower resolutions (∼3.5−3.8 Å). Herein, we report the syntheses of new mixed-oxidation manganese(II/III) compounds based on a tetradentate $N_2O_2$ ligand $H_2L$ and various carboxylates, namely, benzoate, propionate, and pivalate, as ancillary ligands (Scheme 1) that lead respectively to tetra-, tri-, and mononuclear complexes, noted as **1**, **2**, and **3** in the following. X-ray crystallography, electronic and EPR spectroscopic properties, redox behavior, and magnetic susceptibility measurements have been carried out to characterize these compounds.

**Scheme 1**

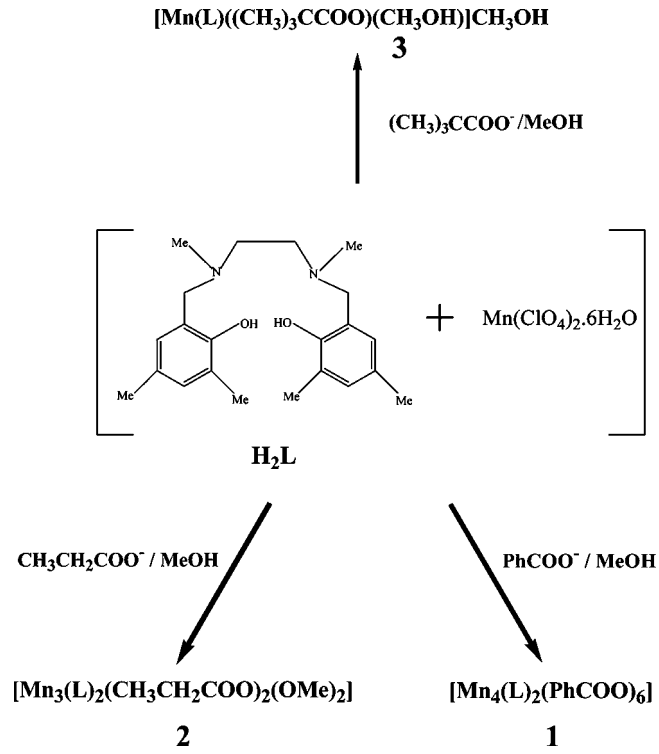


## Experimental Section

**Materials.** The tetradentate ligand *N*,*N*′-dimethyl-*N*,*N*′-bis(2-hydroxy-3,5-dimethylbenzyl)ethylenediamine ($H_2L$; Scheme 1) was prepared according to a reported method.[31] All other reagents were available commercially and used as received. Solvents were reagent-grade, dried from appropriate reagents and distilled under nitrogen prior to their use.[32]

**Preparation of Complexes. $[Mn_4(L)_2(PhCOO)_6]$, 1.** A mixture of $Mn(ClO_4)_2 \cdot 6H_2O$ (0.37 g, 1 mmol) and $H_2L$ (0.36 g, 1 mmol)


(3) Miyasaka, H.; Nakata, K.; Lecren, L.; Coulon, C.; Nakazawa, Y.; Fujisaki, T.; Sugiura, K.; Yamashita, M.; Clérac, R. *J. Am. Chem. Soc.* **2006**, *128*, 3770, and references therein.
(4) Yachandra, V. K.; Sauer, K.; Klein, M. P. *Chem. Rev.* **1996**, *96*, 2927.
(5) Yachandra, V. K.; Derose, V. J.; Latimer, M. J.; Mukherji, I.; Sauer, K.; Klein, M. P. *Science* **1993**, *260*, 675.
(6) Zouni, A.; Witt, H.-T.; Kern, J.; Fromme, P.; Krauβ, N.; Saenger, W.; Orth, P. *Nature (London)* **2001**, *409*, 739.
(7) Kamiya, N.; Shen, J.-R. *Proc. Natl. Acad. Sci. U. S. A.* **2003**, *100*, 98.
(8) Ferreira, K. N.; Iverson, T. M.; Maghlaoui, K.; Barber, J.; Iwata, S. *Science* **2004**, *303*, 1831.
(9) Britt, R. D.; Peloquin, J. M.; Campbell, K. A. *Annu. Rev. Biophys. Biomol. Struct.* **2000**, *29*, 463.
(10) Peloquin, J. M.; Campbell, K. A.; Randall, D. W.; Evanchik, M. A.; Pecoraro, V. L.; Armstrong, W. H.; Britt, R. D. *J. Am. Chem. Soc.* **2000**, *122*, 10926.
(11) (a) Stibrany, R. T.; Gorun, S. M. *Angew. Chem., Int. Ed. Engl.* **1990**, *29*, 1156. (b) Gorun, S. M.; Stibrany, R. T.; Lillo, A. *Inorg. Chem.* **1998**, *37*, 836.
(12) Chen, H.; Faller, J. W.; Crabtree, R. H.; Brudvig, G. W. *J. Am. Chem. Soc.* **2004**, *126*, 7345.
(13) Chan, M. K.; Armstrong, W. H. *J. Am. Chem. Soc.* **1991**, *113*, 5055.
(14) Philouze, C.; Blondin, G.; Menage, S.; Auger, N.; Girerd, J. J.; Vigner, D.; Lance, M.; Nierlich, M. *Angew. Chem., Int. Ed. Engl.* **1992**, *31*, 1629.
(15) (a) Suzuki, M.; Hayashi, Y.; Munezawa, K.; Suenaga, H. S.; Uehara, A. *Chem. Lett.* **1991**, 1929. (b) Suzuki, M.; Sugisawa, T.; Senda, H.; Oshio, H.; Uehara, A. *Chem. Lett.* **1989**, 1091.
(16) (a) Wang, S.; Wemple, M. S.; Yoo, J.; Folting, K.; Huffman, J. C.; Hagen, K. S.; Hendrickson, D. N.; Christou, G. *Inorg. Chem.* **2000**, *39*, 1501. (b) Beedle, C. C.; Stephenson, C. J.; Heroux, K. J.; Wernsdorfer, W.; Hendrickson, D. N. *Inorg. Chem.* **2008**, *47*, 10798.
(17) Mikata, Y.; Wakamatsu, M.; So, H.; Abe, Y.; Mikuriya, M.; Fukui, K.; Yano, S. *Inorg. Chem.* **2005**, *44*, 7268.
(18) (a) Dubé, C. E.; Wright, D. W.; Armstrong, W. H. *Angew. Chem., Int. Ed.* **2000**, *39*, 2169. (b) Visser, H.; Dubé, C. E.; Armstrong, W. H.; Sauer, K.; Yachandra, V. K. *J. Am. Chem. Soc.* **2002**, *124*, 11008. (c) Mukhopadhyay, S.; Staples, R. J.; Armstrong, W. H. *J. Chem. Soc., Chem. Commun.* **2002**, 864. (d) Mukhopadhyay, S.; Mok, H. J.; Staples, R. J.; Armstrong, W. H. *J. Am. Chem. Soc.* **2004**, *126*, 9202.
(19) (a) Yoo, J.; Yamaguchi, A.; Nakano, M.; Krzystek, J.; Streib, W. E.; Brunel, L. C.; Ishimoto, H.; Christou, G.; Hendrickson, D. N. *Inorg. Chem.* **2001**, *40*, 4604. (b) Sanudo, E. C.; Grillo, V. A.; Knapp, M. J.; Bollinger, J. C.; Huffman, J. C.; Hendrickson, D. N.; Christou, G. *Inorg. Chem.* **2002**, *41*, 2441.
(20) (a) Ruettinger, W.; Yagi, M.; Wolf, K.; Bernasek, S.; Dismukes, G. C. *J. Am. Chem. Soc.* **2000**, *122*, 10353. (b) Maneiro, M.; Ruettinger, W. F.; Bourles, E.; McLendon, G. L.; Dismukes, G. C. *Proc. Natl. Acad. Sci. U. S. A.* **2003**, *100*, 3707. (c) Wu, J.-Z.; Sellitto, E.; Yap, G. P. A.; Sheats, J.; Dismukes, G. C. *Inorg. Chem.* **2004**, *43*, 5795.
(21) Boskovic, C.; Bircher, R.; Tregenna-Piggoff, P. L. W.; Gudel, H. U.; Paulsen, C.; Wernsdorfer, W.; Barra, A.-L.; Khatsko, E.; Neels, A.; Stoeckli-Evans, H. *J. Am. Chem. Soc.* **2003**, *125*, 14046.
(22) Hewitt, I. J.; Tang, J.-K.; Madhu, N. T.; Clérac, R.; Buth, G.; Anson, C. E.; Powell, A. K. *Chem. Commun.* **2006**, 2650.
(23) Tangoulis, V.; Malamatari, D. A.; Spyroulins, G. A.; Raptopoulou, C. P.; Terzis, A.; Kessissoglou, D. P. *Inorg. Chem.* **2000**, *39*, 2621.
(24) Hirotsu, M.; Aoyagi, M.; Kojima, M.; Mori, W.; Yoshikawa, Y. *Bull. Chem. Soc. Jpn.* **2002**, *75*, 259.
(25) Milios, C. J.; Stamatatos, T. C.; Kyritsis, P.; Terzis, A.; Raptopoulou, C. P.; Vicente, R.; Escuer, A.; Perlepes, S. P. *Eur. J. Inorg. Chem.* **2004**, 2885.
(26) Asada, H.; Hayashi, K.; Negoro, S.; Fujiwara, M.; Matsushita, T. *Inorg. Chem. Commun.* **2003**, *6*, 193.
(27) Bhaduri, S.; Pink, M.; Christou, G. *Chem. Commun.* **2002**, 2352.
(28) Canada-Vilalta, C.; Streib, W. E.; Huffman, J. C.; O'Brian, T. A.; Davidson, E. R.; Christou, G. *Inorg. Chem.* **2004**, *43*, 101.
(29) Hirotsu, M.; Kojima, M.; Yoshikawa, Y. *Bull. Chem. Soc. Jpn.* **1997**, *70*, 649.
(30) Chai, J.; Zhu, H.; Roesky, H. W.; Yang, Z.; Jancik, V.; Herbst-Irmer, R.; Schmidt, H.-G.; Noltemeyer, M. *Organometallics* **2004**, *23*, 5003.
(31) Mialane, P.; Mallart, A.; Blondin, G.; Nivorojkine, A.; Guilhem, J.; Tchertanova, L.; Cesario, M.; Ravi, N.; Bominaar, E.; Girerd, J.; Munck, E. *Inorg. Chim. Acta* **1997**, *263*, 367.

in MeOH (25 mL) was allowed to stir for 30 min at room temperature, affording a clear green solution. To this was added sodium benzoate (0.22 g, 1.5 mmol) in solid form, and the mixture was stirred further for 1 h. The resulting green solution was rotary evaporated to a ca. 10 mL volume and kept in a refrigerator at ca. 4 °C for 3 days. A dark crystalline compound along with single crystals was obtained. Yield: 0.11 g (27%). Anal. calcd for $C_{86}H_{90}N_4O_{16}Mn_4$: C, 62.40; H, 5.48; N, 3.38. Found: C, 61.98; H, 5.34; N, 3.21%. IR (KBr disk, $cm^{-1}$): 3436, 2926, 1605, 1552, 1471, 1404, 1242, 720. UV−vis ($CH_2Cl_2$) [$\lambda_{max}$/nm ($\varepsilon$/$mol^{-1}cm^2$)]: 595 (5800), 436 (5850), 272 (28 300). $\mu_{eff}$ = 11.0 $\mu_B$ at 25 °C.

**$[Mn_3(L)_2(CH_3CH_2COO)_2(OMe)_2]\cdot H_2O$, 2.** This compound was prepared following an analogous procedure to that mentioned above for **1** using sodium propionate as an ancillary carboxylate ligand. Yield: 35%. Anal. calcd for $C_{52}H_{78}N_4O_{11}Mn_3$: C, 56.78; H, 7.15; N, 5.09. Found: C, 57.30; H, 6.95; N, 5.08%. IR (KBr disk, $cm^{-1}$): 3420, 2914, 1565, 1471, 1419, 1251, 1038, 859, 815. UV−vis ($CH_2Cl_2$) [$\lambda_{max}$/nm ($\varepsilon$/$mol^{-1}cm^2$)]: 563 (2550), 282 (15 900), 249 (22 000). $\mu_{eff}$ = 8.9 $\mu_B$ at 25 °C.

**$[Mn(L)\{(CH_3)_3CCOO\}(CH_3OH)]\cdot CH_3OH$, 3.** An analogous method of preparation to that described above for **1** was employed using sodium pivalate as a replacement for benzoate. The resulting green solution was reduced to a ca. 10 mL volume using a rotary evaporator and kept in the open air for crystallization. A dark crystalline compound along with single crystals was obtained. Yield: 50%. Anal. calcd for $C_{29}H_{47}MnN_2O_6$: C, 60.62; H, 8.18; N, 4.87. Found: C, 61.10; H, 7.85; N, 5.20%. IR (KBr disk, $cm^{-1}$): 3591, 3420, 2917, 1550, 1474, 1410 1254, 831, 627. UV−vis ($CH_2Cl_2$) [$\lambda_{max}$/nm ($\varepsilon$/$mol^{-1}cm^2$)]: 554 (1950), 373 (4500), 287 (10 600), 248 (15 300). $\mu_{eff}$ = 4.5 $\mu_B$ at 25 °C.

**Physical Measurements.** IR spectroscopic measurements were done on samples pressed into KBr discs using a Nicolet 520 FTIR spectrometer. Electronic spectra in solution were recorded on a Perkin-Elmer model Lambda 950 UV−vis−NIR spectrophotometer. The X-band EPR spectra were recorded on a Bruker model ELEXSYS E500 spectrometer equipped with a He flow cryostat (Oxford Instruments ESR910). Elemental analyses (for C, H, and N) were performed in our laboratory (at IACS) using a Perkin-Elmer model 2400 Series II elemental analyzer.

Magnetic measurements were performed on polycrystalline samples in the temperature range 1.8−300 K on a Quantum Design MPMS-XL SQUID magnetometer. The samples of **1** and **2** were packed in a sealed plastic bag. The raw data were corrected for the sample holder and the orbital diamagnetic contributions calculated from Pascal's constant.[33] The samples have been checked for ferromagnetic impurities, which were found to be absent by measuring the field dependence of the magnetization at $T$ = 100 K.

The cyclic voltammetric measurements were performed at 25 °C under purified dinitrogen using a Bioanalytical Systems BAS 100B electrochemical analyzer. The concentration of the supporting electrolyte tetrabutylammonium perchlorate (TBAP) was 0.1 M, while that of the complex was 1 mM. A three-electrode assembly comprising a platinum disk working electrode, a platinum wire counter electrode, and an aqueous Ag/AgCl reference electrode was used. IR compensation was made automatically during each run. Under the experimental conditions used, the $E_{1/2}$ value for the ferrocene/ferrocenium couple was 440 mV.

**X-Ray Crystallography.** Diffraction-quality crystals of **1** (blue plate, 0.30 × 0.22 × 0.09 mm), **2** (black block, 0.43 × 0.30 × 0.16 mm), and **3** (green prism, 0.34 × 0.28 × 0.22 mm) were grown from the reaction pots as described in the Experimental Section. Intensity data for compounds **1** and **2** were measured on a Bruker SMART 1000 CCD diffractometer using graphite-monochromated Mo Kα ($\lambda$ = 0.71073 Å) radiation in the $\omega-2\theta$ scan mode at 293 K. For compound **3**, a similar mode of data collection was carried out at 100 K using a Bruker AXS SMART APEX II CCD Diffractometer. Accurate cell parameters and orientation matrices were determined from setting angles of 2413, 7377, and 5469 reflections in the ranges 2.3415° ≤ $\theta$ ≤ 19.852°, 2.246° ≤ $\theta$ ≤ 26.8025°, and 1.26° ≤ $\theta$ ≤ 25.88° for **1**, **2**, and **3**, respectively. No crystal decay was observed during the data collections. The intensity data were corrected for empirical absorption. In all cases, absorption corrections based on multiscan using the SADABS software[34] were applied. The structures were solved by direct methods[35] and refined on $F^2$ by a full-matrix least-squares procedure[35] with anisotropic displacement parameters for all of the non-hydrogen atoms (except for the C(41) and C(42) atoms in **1**) based on all data minimizing $wR = [\sum[w(F_0^2 - F_c^2)^2]/\sum(F_0^2)^2]^{1/2}$, $R = \sum ||F_0| - |F_c||/\sum |F_0|$, and

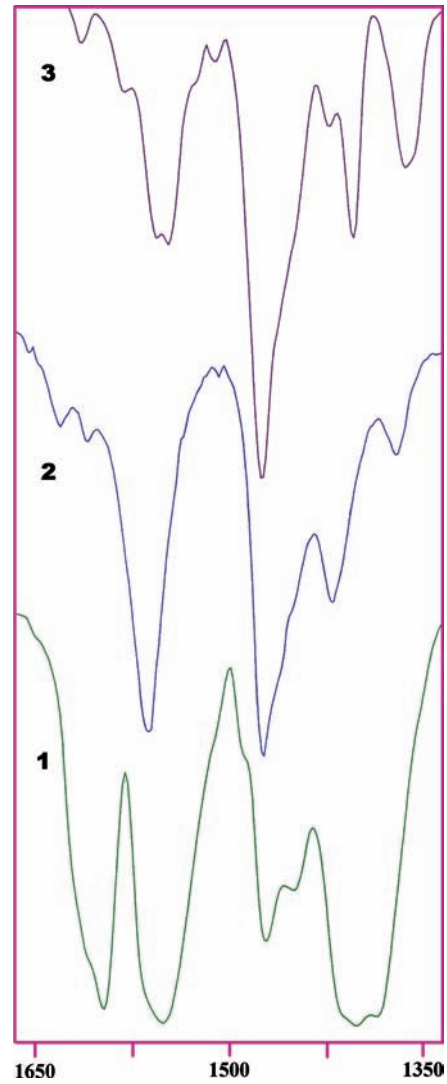


**Figure 1.** Relevant region (1350−1650 $cm^{-1}$) of the IR spectra (in KBr disk) for compounds **1**, **2**, and **3** showing the characteristic split patterns in the $\nu(COO^-)$ stretching modes.

(32) Perrin, D. D.; Armarego, W. L. F.; Perrin, D. R. *Purification of Laboratory Chemicals*, 2nd ed.; Pergamon: Oxford, 1980.

(33) *Theory and Applications of Molecular Paramagnetism*; Boudreaux, E. A., Mulay, L. N., Eds.; John Wiley & Sons: New York, 1976.

(34) Sheldrick, G. M. *SADABS*; University of Göttingen: Göttingen, Germany, 1996.

(35) SHELXS-97: Sheldrick, G. M. *Acta Crystallogr.* **1990**, *46A*, 467.

**Table 1.** Summary of the Crystallographic Data for the Complexes **1**, **2**, and **3**

| | **1** | **2** | **3** |
|---|---|---|---|
| formula | $C_{86}H_{90}Mn_4N_4O_{16}$ | $C_{52}H_{78}Mn_3N_4O_{11}$ | $C_{29}H_{46}MnN_2O_6$ |
| $T$ (K) | 293(2) | 293(2) | 100(2) |
| fw | 1655.38 | 1100 | 573.62 |
| cryst size ($mm^3$) | 0.300 × 0.220 × 0.090 | 0.432 × 0.299 × 0.162 | 0.34 × 0.28 × 0.22 |
| cryst syst | monoclinic | triclinic | monoclinic |
| space group | $P2_1/c$ | $P1$ | $P2_1/c$ |
| $a$ (Å) | 11.9415(8) | 10.9271(9) | 16.274(3) |
| $b$ (Å) | 20.3663(14) | 11.6090(10) | 12.502(2) |
| $c$ (Å) | 17.0596(12) | 13.2060(11) | 14.354(3) |
| α (deg) | 90 | 65.9610(10) | 90 |
| $\beta$ (deg) | 101.0580(2) | 83.0920(10) | 95.224(5) |
| $\gamma$ (deg) | 90 | 63.9420(10) | 90 |
| $V$ ($A^3$) | 4071.9(5) | 1370.9(2) | 2908.2(10) |
| $Z$ | 2 | 1 | 4 |
| $\rho_{calcd}$ ($Mg/M^3$) | 1.350 | 1.332 | 1.310 |
| $\lambda$(Mo Kα) (Å) | 0.71073 | 0.71073 | 0.71073 |
| $\mu$ ($mm^{-1}$) | 0.674 | 0.740 | 0.497 |
| $2\theta_{max}$ (deg) | 56.30 | 56.70 | 51.76 |
| no. ind. reflns, total | 10075 | 13364 | 19592 |
| obsd [$I \geq 2\sigma(I)$] | 3843 | 10898 | 4338 |
| $R_{int}$ | 0.0915 | 0.0185 | 0.0446 |
| no. params | 486 | 640 | 480 |
| R1($F_0$), wR2($F_0$) [$I \geq 2\sigma(I)$] | 0.0589, 0.1377 | 0.0381, 0.090 | 0.0617, 0.1371 |
| $F$(000)/GOF on $F^2$ | 1724/0.958 | 581/1.016 | 1228/1.162 |

$S = [\sum[w(F_0^2 - F_c^2)^2]/(n - p)]^{1/2}$. SHELXL-97 was used for both structure solutions and refinements.[36] Hydrogen atoms were geometrically calculated and isotropically fixed at positions recalculated after each cycle of refinement [$d$(C−H) = 0.95 Å, with the isotropic thermal parameter of $U_{iso}$(H) = 1.2$U_{iso}$(C)]. In compound **3**, precise determination of the location of the hydrogen bound to the coordinated oxygen atom of methanol was not possible. The structures of **2** and **3**, based on Fourier difference maps calculated toward the end of each refinement, indicated the presence of residual electron density peaks, consistent with the solvent molecules of crystallization. For **2**, these were satisfactorily modeled as a single water molecule disordered over two positions, OW1 and OW1A, with a 50% site occupancy factor for each. For **3**, on the other hand, it turns out to be a methanol molecule with 100% occupancy. The SMART and SAINT-plus software packages[37] were used for data collection and reduction, respectively. Figures 2−4 were drawn with the DIAMOND program.[38] Crystals parameters and the details of the data collections and refinements are summarized in Table 1.

## Results and Discussion

**Syntheses.** Mono- and multinuclear manganese(II/III) complexes (**1**−**3**) have been synthesized using $H_2L$ as a facially coordinating sterically constrained $N_2O_2$ ligand. The detailed strategy is summarized in Scheme 1. The reactions have been carried out in methanol at room temperature in the presence of sodium salts of the ancillary carboxylate ligands and $Mn(ClO_4)_2 \cdot 6H_2O$ as the metal ion precursor. During the course of these reactions, manganese(II) is partially or completely oxidized to manganese(III) by atmospheric oxygen. With an ancillary benzoate ligand, the product obtained is a tetranuclear mixed-valence species $[Mn^{II}_2Mn^{III}_2(L)_2(PhCOO)_6]$, **1**, with symmetrical valence distribution, $Mn^{III}-Mn^{II}_2-Mn^{III}$, thus paving its way into a rare group of tetramanganese compounds with a biologically relevant "dimer-of-dimers" structure.[11−16] Interestingly enough, when a propionate ligand is used to replace benzoate in the above reaction protocol, the product obtained is a trinuclear $Mn^{III}/Mn^{II}$ compound $[Mn^{III}_2Mn^{II}(L)_2(CH_3CH_2COO)_2(OMe)_2] \cdot H_2O$, **2**, as revealed from X-ray crystallography (vide infra). With bulky pivalate, on the other hand, the product isolated is a mononuclear manganese(III) compound, $[Mn(L)\{(CH_3)_3CCOO\}(CH_3OH)] \cdot CH_3OH$, **3**. Apart from their bulkiness, the electronic influence (basicity) of the carboxylates as ancillary ligands plays a pivotal role in deciding the nuclearity of the final product. Thus, pivalate and benzoate being the most and least electron-donating, respectively, the higher basicity of pivalate gives rise to the hydrogen bond with the coordinated methanol, thus stabilizing the mononuclear structure in compound **3**. The other carboxylates are engaged in the bridging structures of **1** and **2** just to compensate for the lack of this effect. Also, the prime ligand $H_2L$ due to its sufficiently flexible backbone is acting like a capping ligand in these complexes. The use of Schiff base ligands with a $N_2O_2$ donor set, however, generates manganese(III) complexes with salen-type dimeric octahedral structures[39,40] in which the $N_2O_2$ ligands occupy the equatorial plane because of their structural rigidity. Compounds **1**−**3** are air-stable in the solid state. In solution, also, these are fairly stable and undergo slow decomposition only upon prolonged standing for more than 12 hours.

IR spectra of complexes **1**−**3** display characteristic bands of the coordinated tetradentate ligand. One such prominent band appears at ca. 1250 $cm^{-1}$ due to $\upsilon$(C−O/phenolate) stretchings. Of particular interest here are the appearances of strong bands in the 1650−1350 $cm^{-1}$ region due to different modes of carboxylate vibrations, as shown in Figure

(36) Sheldrick, G. M. *SHELXL-97*, release 97-1; University of Gottingen: Gottingen, Germany, 1997.
(37) *SAINT-plus, Software Users Guide*, version 6.0; Bruker Analytical X-ray Systems: Madison, WI, 1999.
(38) *DIAMOND, Visual Crystal Structure Information System*, version 3.1; CRYSTAL IMPACT: Bonn, Germany, 2004.
(39) Kachi-Terajima, C.; Miyasaka, H.; Sugiura, K.-I.; Clérac, R.; Nojiri, H. *Inorg. Chem.* **2006**, *45*, 4381.
(40) Clérac, R.; Miyasaka, H.; Yamashita, M.; Coulon, C. *J. Am. Chem. Soc.* **2002**, *124*, 12837.

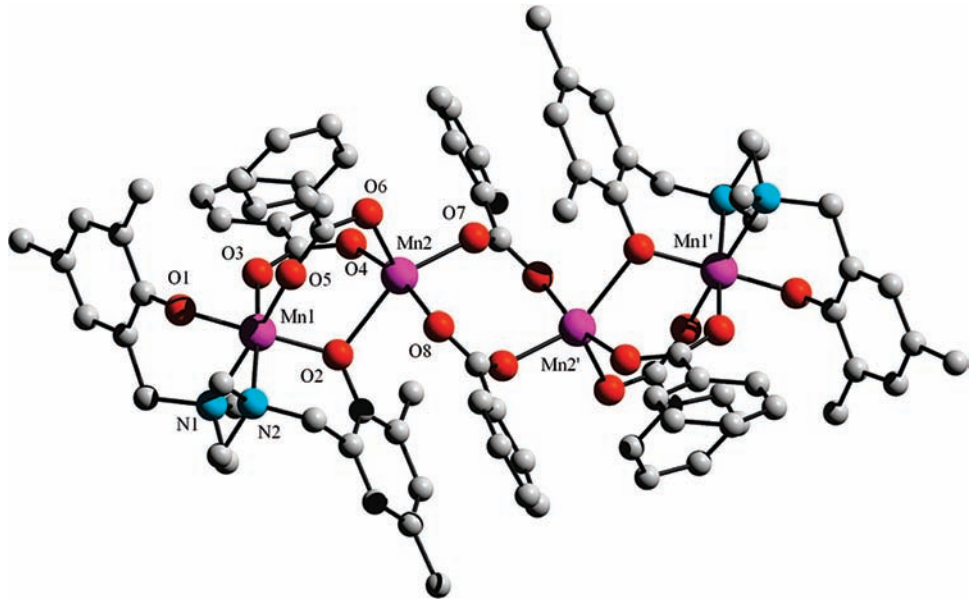


**Figure 2.** Molecular structure for complex **1** with the atom numbering scheme.

1. A strong two-band pattern, observed for **2** at 1564 and 1421 $cm^{-1}$ due to $\upsilon_a(COO^-)$ and $\upsilon_s(COO^-)$ vibrations, respectively, is as expected for a bis-monodentate bridging mode of carboxylate binding.[41] In the case of **1**, however, four such carboxylate stretchings are observed at 1597, 1553, 1402, and 1387 $cm^{-1}$. Taking cues from the results of X-ray diffraction analysis (see later), one can explain these data as arising from a pair of $\upsilon_a(COO^-)$ and $\upsilon_s(COO^-)$ vibrations originating from the two different types of carboxylate bridging, one that connects two trapped-valence manganese centers ($Mn^{II}$ and $Mn^{III}$) through a syn−syn mode while the other is between two isovalent manganese(II) centers through syn−anti attachment. In **3**, a single carboxylate group is present in a syn−syn-type bridging mode between the lone metal center and a hydrogen atom of the coordinated methanol molecule, thus generating a two-band pattern at 1550 and 1410 $cm^{-1}$, similar to what has been observed with **2**. It is worth noting that the IR spectrum of **2** also contains a strong band at 1038 $cm^{-1}$, indicating the presence of bridging methoxy groups.

**Description of Crystal Structures.** The molecular structure of **1** is shown in Figure 2. Its important interatomic parameters are listed in Table 2. The complex crystallizes in a monoclinic space group, $P2_1/c$, with two molecular weight units per cell. A crystallographic inversion center is located at the center of this tetranuclear complex that generates two crystallographically equivalent dinuclear units, connected together by a pair of syn−anti bridging benzoates that link Mn(2) and Mn(2)′ atoms. This compound is thus a rare example of a mixed-valence tetramanganese compound with a "dimer-of-dimers" structural pattern.[11−16] Each dimeric unit consists of a trapped-valence $Mn^{III}$−$Mn^{II}$ core [Mn(1)−Mn(2)], involving a tetragonally distorted terminal $Mn^{III}$ center (Mn1) in the midst of a distorted octahedral geometry, comprised of the donor atoms O(1), N(1), N(2), and O(2), all coming from the tetradentate ligand, together with O(3) and O(5) atoms from the bridging benzoates. The trans angles O(1)−Mn(1)−O(2), N(1)−Mn(1)−O(5), and O(3)−Mn(1)−N(2) are 179.16(14)°, 167.81(14)°, and 173.51(14)°, respectively. The bond distances Mn(1)−O(1) (1.858(3) Å), Mn(1)−O(2) (1.920(3) Å), Mn(1)−N(2) (2.160(3) Å), and Mn(1)−O(3) (1.971(3) Å) are as expected for $Mn^{III}$−O(phenoxo), 1.860−1.884 Å;[24,42,43] $Mn^{III}$−O-($\mu$−phenoxo), 1.920(3) Å;[24] $Mn^{III}$−N(imino), 2.090(4)−2.111(2) Å;[17,24] and $Mn^{III}$−O(carboxylato), 1.890(3)−1.985(2) Å,[42,43] bonds, respectively. The remaining two bonds Mn(1)−O(5) (2.160(3) Å) and Mn(1)−N(1) (2.336(4) Å) are significantly enlarged and may be considered as axially

**Table 2.** Selected Bond Distances (Å) and Angles (deg) for **1**

| Bond Distances (Å) | | | |
|---|---|---|---|
| Mn(1)−O(1) | 1.858(3) | Mn(1)−O(2) | 1.920(3) |
| Mn(1)−O(3) | 1.971(3) | Mn(1)− O(5) | 2.160(3) |
| Mn(1)−N(2) | 2.160(3) | Mn(1)−N(1) | 2.336(4) |
| Mn(2)−O(7) | 2.063(4) | Mn(2)−O(6) | 2.098(4) |
| Mn(2)−O(8) | 2.111(3) | Mn(2)−O(4) | 2.127(3) |
| Mn(2)−O(2) | 2.258(3) | | |
| **Bond Angles (deg)** | | | |
| O(1)−Mn(1)−O(2) | 179.16(14) | O(1)−Mn(1)−O(3) | 89.65(13) |
| O(2)−Mn(1)−O(3) | 90.19(13) | O(1)−Mn(1)−O(5) | 89.46(14) |
| O(2)−Mn(1)−O(5) | 89.74(14) | O(3)−Mn(1)−O(5) | 97.79(14) |
| O(1)−Mn(1)−N(2) | 89.57(14) | O(2)−Mn(1)−N(2) | 90.68(13) |
| O(3)−Mn(1)−N(2) | 173.51(14) | O(5)−Mn(1)−N(2) | 88.65(14) |
| O(1)−Mn(1)−N(1) | 84.66(14) | O(2)−Mn(1)−N(1) | 96.17(14) |
| O(3)−Mn(1)−N(1) | 92.86(14) | O(5)−Mn(1)−N(1) | 167.81(14) |
| N(2)−Mn(1)−N(1) | 80.65(14) | O(7)−Mn(2)−O(6) | 106.03(16) |
| O(7)−Mn(2)−O(8) | 100.36(14) | O(6)−Mn(2)−O(8) | 90.95(15) |
| O(7)−Mn(2)−O(4) | 87.36(14) | O(6)−Mn(2)−O(4) | 97.09(16) |
| O(8)−Mn(2)−O(4) | 166.91(14) | O(7)−Mn(2)−O(2) | 140.47(14) |
| O(6)−Mn(2)−O(2) | 112.91(14) | O(8)−Mn(2)−O(2) | 85.85(11) |
| O(4)−Mn(2)−O(2) | 81.53(12) | | |

(41) Nakamoto, K. *Infrared and Raman Spectra of Inorganic and Coordination Compounds*, 3rd ed.; Wiley-Interscience: New York, 1978.

(42) Kessissoglou, D. P.; Kirk, M. L.; Lah, M. S.; Li, X.; Raptopoulou, C.; Hatfield, W. E.; Pecoraro, V. L. *Inorg. Chem.* **1992**, *31*, 5424.

(43) Tangoulis, V.; Malamatari, D. A.; Soulti, K.; Stergiou, V.; Raptopoulou, C. P.; Terzis, A.; Kabanos, T. A.; Kessissoglou, D. P. *Inorg. Chem.* **1996**, *35*, 4974.

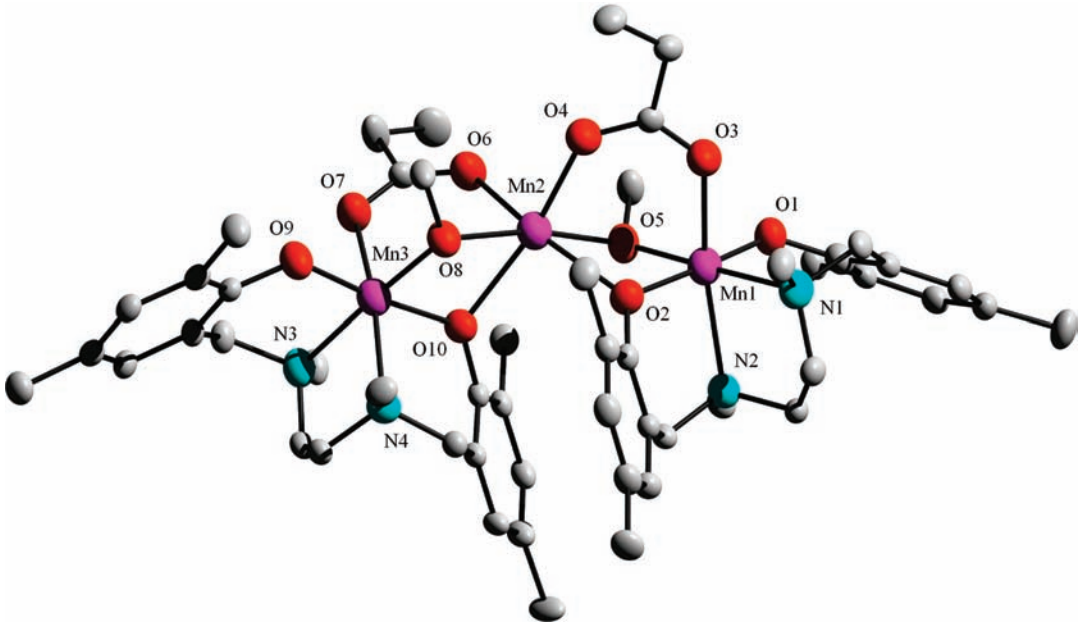


**Figure 3.** Molecular structure for complex **2** with the atom numbering scheme.

elongated bonds due to Jahn−Teller distortion.[44] The $Mn^{II}$ centers in this molecule adopt trigonal-bipyramidal geometry with three basal positions being occupied by the carboxylato oxygen atoms O(6) and O(7) and the bridging phenolate oxygen O(2). The axial positions are taken by O(4) and O(8) atoms belonging to another pair of carboxylate moieties. The trans angle O(8)−Mn(2)−O(4) is 166.91(14)°, while the Mn(2)−O(carboxylate) distances (2.063(4)−2.127(3) Å) and the Mn(2)−O(2)($\mu$-phenoxo) distance (2.258(3) Å) are in the expected ranges.[24,42,43] Of particular interest here is the systematically larger metal ion to donor atom distances for the Mn(2) center compared to the corresponding distances for the Mn(1) coordination sphere. Results actually confirm the trapped-valence nature of this mixed oxidation compound in which the terminal $Mn^{III}$ and the central $Mn^{II}$ are separated [Mn(1)···Mn(2)] by 3.434(12) Å. This trapped-valence dimer is connected to another similar dimer through a pair of syn−anti carboxylate bridges (Figure 2). The Mn(2)···Mn(2)′ and Mn(1)···Mn(2)′ separations in this molecule are 4.224(20) Å and 7.240(13) Å, respectively.

The molecular structure of **2** is shown in Figure 3 and the selected bond distances and angles in Table 3. Like **1**, trinuclear compound **2** also has a grossly linear trapped-valence structure involving a mixed-oxidation $Mn^{III}−Mn^{II}−Mn^{III}$ [Mn(1)−Mn(2)−Mn(3)] core. The central Mn(2) has a distorted octahedral geometry comprised of two syn−syn bridging propionates providing the donors O(6) and O(4) and two methoxy oxygen atoms O(8) and O(5) together with a pair of bridging phenoxy oxygen atoms O(10) and O(2), coming from the tetradentate $N_2O_2$ ligands. The basal positions are taken up by O(2), O(4), O(6), and O(10) oxygen atoms, while the axial sites are taken up by O(8) and O(5) atoms. The trans angles O(8)−Mn(2)−O(5), O(10)−Mn(2)−O(4), and O(2)−Mn(2)−O(6) are 169.94(8)°, 165.80(8)°, and 162.42(8)°, respectively. The central $Mn^{II}$ is flanked by two terminal $Mn^{III}$ ions with distorted octahedral geometry, each composed of a facially coordinating $N_2O_2$ ligand, providing O(9), N(3), N(4), and O(10) donor atoms to Mn(3) (corresponding donor atoms for Mn(1) are O(1), N(1), N(2), and O(2), respectively) along with a bridging methoxy oxygen O(8) (O(5)) and a syn−syn bridging carboxylate oxygen O(7) (O(3)). The valence-trapped structures of these Jahn−Teller distorted $Mn^{III}$ centers have been confirmed in a comparison of the bond length data (Table 3), where Mn(2) ligand

**Table 3.** Relevant Bond Distances (Å) and Angles (deg) for **2**

| | | | |
|---|---|---|---|
| Bond Distances (Å) | | | |
| Mn(1)−O(1) | 1.892(2) | Mn(1)−O(5) | 1.911(2) |
| Mn(1)−O(2) | 1.946(2) | Mn(1)−O(3) | 2.164(2) |
| Mn(1)−N(1) | 2.177(2) | Mn(1)−N(2) | 2.332(2) |
| Mn(2)−O(4) | 2.129(2) | Mn(2)−O(8) | 2.154(2) |
| Mn(2)−O(5) | 2.156(2) | Mn(2)−O(6) | 2.162(2) |
| Mn(2)−O(2) | 2.280(2) | Mn(2)−O(10) | 2.2549(19) |
| Mn(3)−O(9) | 1.873(2) | Mn(3)−O(10) | 1.9255(18) |
| Mn(3)−N(3) | 2.191(2) | Mn(3)−O(7) | 2.195(2) |
| Mn(3)−O(8) | 1.921(2) | Mn(3)−N(4) | 2.316(2) |
| Bond Angles (deg) | | | |
| O(1)−Mn(1)−O(5) | 89.96(9) | O(1)−Mn(1)−O(2) | 172.29(9) |
| O(5)−Mn(1)−O(2) | 82.61(8) | O(1)−Mn(1)−O(3) | 92.19(9) |
| O(5)−Mn(1)−O(3) | 92.52(9) | O(2)−Mn(1)−O(3) | 90.19(8) |
| O(1)−Mn(1)−N(1) | 90.66(9) | O(5)−Mn(1)−N(1) | 178.34(10) |
| O(2)−Mn(1)−N(1) | 96.83(9) | O(3)−Mn(1)−N(1) | 85.92(9) |
| O(1)−Mn(1)−N(2) | 92.22(8) | O(5)−Mn(1)−N(2) | 101.97(9) |
| O(2)−Mn(1)−N(2) | 87.35(8) | O(3)−Mn(1)−N(2) | 164.86(8) |
| N(1)−Mn(1)−N(2) | 79.55(9) | O(4)−Mn(2)−O(8) | 96.15(8) |
| O(4)−Mn(2)−O(5) | 92.31(8) | O(8)−Mn(2)−O(5) | 169.94(8) |
| O(5)−Mn(2)−O(6) | 92.50(8) | O(4)−Mn(2)−O(10) | 165.80(8) |
| O(8)−Mn(2)−O(10) | 69.67(7) | O(5)−Mn(2)−O(10) | 101.87(7) |
| O(6)−Mn(2)−O(10) | 83.82(8) | O(4)−Mn(2)−O(2) | 86.36(8) |
| O(8)−Mn(2)−O(2) | 105.06(8) | O(5)−Mn(2)−O(2) | 69.99(7) |
| O(6)−Mn(2)−O(2) | 162.42(8) | O(10)−Mn(2)−O(2) | 97.80(7) |
| O(9)−Mn(3)−O(8) | 91.51(9) | O(4)−Mn(2)−O(6) | 96.32(9) |
| O(8)−Mn(3)−O(10) | 81.85(8) | O(9)−Mn(3)−o(10) | 173.22(9) |
| O(8)−Mn(3)−N(3) | 176.85(9) | O(9)−Mn(3)−N(3) | 91.51(9) |
| O(9)−Mn(3)−O(7) | 90.31(9) | O(10)−Mn(3)−N(3) | 95.15(8) |
| O(10)−Mn(3)−O(7) | 88.81(8) | O(8)−Mn(3)−O(7) | 94.06(9) |
| O(9)−Mn(3)−N(4) | 94.60(9) | N(3)−Mn(3)−O(7) | 86.80(9) |
| O(10)−Mn(3)−N(4) | 87.87(8) | O(8)−Mn(3)−N(4) | 99.41(9) |
| O(7)−Mn(3)−N(4) | 165.52(8) | N(3)−Mn(3)−N(4) | 79.47(9) |

(44) Goodson, P. A.; Oki, A. R.; Glerup, J.; Hodgson, D. J. *J. Am. Chem. Soc.* **1990**, *112*, 6248.

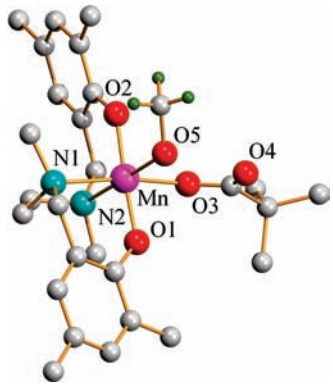


**Figure 4.** Molecular structure for complex **3** with the atom numbering scheme.

distances in the basal plane are systematically larger than the corresponding distances around Mn(1) and Mn(3). Thus, Mn(2)−O(8) (2.154(2) Å) and Mn(2)−O(5) (2.156(2) Å) distances are longer than Mn(3)−O(8) (1.921(2) Å) and Mn(1)−O(5) distances (1.911(2) Å), respectively. Similar disparities are also observed between the distances Mn(2)−O(10) (2.2549 (19) Å) and Mn(3)−O(10) (1.9255(18) Å), and Mn(2)−O(2) (2.280(2) Å) and Mn(1)−O(2) (1.946(2) Å). The trans angle N(2)−Mn(1)−O(3), 164.86(8)° (165.52(8)°), is showing maximum deviation from linearity as demanded by the Jahn−Teller effect, such that the bond lengths of Mn(1)−N(2), 2.332(2) Å (2.316(2) Å), and Mn(1)−O(3), 2.164(2) Å (2.195(2) Å), are showing distinct elongation compared to relevant basal distances. Thus, the expected difference in Mn(2)−O(4) and Mn(1)−O(3) bond lengths due to valence-trapping is leveled out by Jahn−Teller expansion. Similar opposing influences are also operative on the Mn(3)−O(7) bond (2.195(2) Å) to make it comparable with the Mn(2)−O(6) distance, 2.162(2) Å. The Mn(1)···Mn(3) separation (6.084 Å) in this molecule is less than the sum of the Mn(1)···Mn(2) (3.178 Å) and Mn(2)···Mn(3) separations (3.186 Å), making the molecule more angular in nature [Mn(1)···Mn(2)···Mn(3) angle is 145.89°], as shown in Figure 3. Thus, **2** may be viewed as consisting of two facially coordinating tridentate metalloligands $[LMn^{III}(OCH_3)(CH_3CH_2COO)]^-$, attached to a central $Mn^{II}$ through $\mu$-OPh, $\mu$-$OCH_3$, and syn−syn carboxylate bridges to provide an octahedral geometry that unusually lacks a crystallographic center of symmetry.[23,42,43]

There are some $\pi-\pi$ stacking interactions operative between the two phenolates and two benzoates in **1** and between the two phenolates in **2**. While the two phenolates in **2** are in an eclipsed position, the corresponding orientations in **1** are somewhat intermediate between a staggered and an eclipsed position.

The labeled diagram for **3** is shown in Figure 4, and the relevant metrical parameters are given in Table 4. The complex crystallizes in the monoclinic space group $P2_1/c$ with four molecular weight units/cell. The manganese center in this mononuclear complex is six-coordinated using a doubly deprotonated tetradentate $L^{2-}$ ligand, providing O(1), N(1), N(2), and O(2) donor atoms; a monodentate pivalate, O(3); and a methanol molecule, O(5). The bond distances Mn−N (2.147(3)−2.226(3) Å) and Mn−O (1.847(2)−2.215(3) Å) are all in the expected ranges. The methanol oxygen [O(5)] occupies the Jahn−Teller axis together with N(2) from the imino group of the $L^{2-}$ ligand, to form a trans angle O(5)−Mn−N(2) of 178.63(12)°. The elongation along this axis is clearly reflected in the bond lengths of Mn−N(2), 2.226(3) Å, and Mn−O(5), 2.215(3) Å, compared to relevant bond distances in the equatorial plane (Table 4). Of particular interest here is the monodentate coordination mode of the carboxylate ligand as against the bridging modes, observed in **1** and **2**. Hydrogen bonding plays a dominant role in this molecule in providing extra stability to the monodentate carboxylate group as the noncoordinating oxygen atom O(4) of pivolate remains attached to the alcoholic hydrogen atom of the coordinated methanol. Unfortunately, we are unable to locate precisely the position of that hydrogen atom.

**Table 4.** Selected Bond Distances (Å) and Angles (deg) for **3**

| | | | |
|---|---|---|---|
| Bond Distances (Å) | | | |
| Mn−O(2) | 1.847(2) | Mn−O(1) | 1.852(2) |
| Mn−O(3) | 2.000(3) | Mn−N(1) | 2.147(3) |
| Mn−O(5) | 2.215(3) | Mn−N(2) | 2.226(3) |
| Bond Angles (deg) | | | |
| O(2)−Mn−O(1) | 176.39(11) | O(2)−Mn−O(3) | 92.06(11) |
| O(1)−Mn−O(3) | 86.20(11) | O(2)−Mn−N(1) | 93.21(11) |
| O(1)−Mn−N(1) | 88.95(11) | O(3)−Mn−N(1) | 170.66(12) |
| O(2)−Mn−O(5) | 89.63(10) | O(1)−Mn−N(5) | 87.23(11) |
| O(3)−Mn−O(5) | 90.73(12) | N(1)−Mn−O(5) | 97.01(12) |
| O(2)−Mn−N(2) | 90.27(11) | O(1)−Mn−N(2) | 92.92(11) |
| O(3)−Mn−N(2) | 90.64(12) | N(1)−Mn−N(2) | 81.63(12) |
| O(5)−Mn−N(2) | 178.63(12) | | |

**Magnetism and EPR.** Magnetic susceptibility data for the polycrystalline samples of **1** and **2** have been obtained in the 1.8−300 K temperature range in an applied field of 0.1 T. The $\chi T$ versus $T$ plots for **1** and **2** are displayed in Figure 5. For compound **1**, the room-temperature $\chi T$ value is 15.2 $cm^3$ K $mol^{-1}$, close to the spin-only value ($g = 2.0$) of 14.75 $cm^3$ K $mol^{-1}$, expected for a $Mn^{III}_2Mn^{II}_2$ system in the high-temperature limit in which the metal centers can be considered as magnetically isolated. With decreasing temperature, the $\chi T$ product increases monotonically, first at a slow pace (up to 90 K) and then more rapidly, to reach a value of 31.7 $cm^3$ K $mol^{-1}$ at 1.8 K, thus indicating a dominant ferromagnetic exchange coupling among the paramagnetic metal centers. In order to analyze this magnetic behavior, the coupling topology (including only neighboring interactions) deduced from the crystal structure has to be considered as shown in Scheme 2.

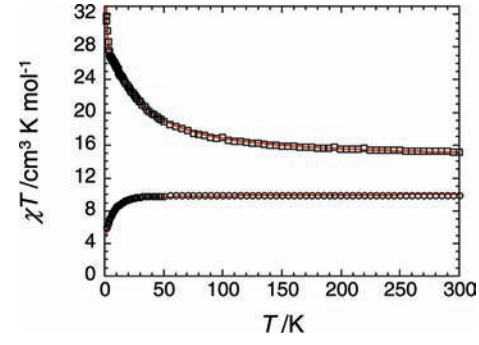


**Figure 5.** Temperature dependence of the $\chi T$ product for **1** (□) and **2** (○) at $H = 0.1$ T. The red lines are the best fits of the data using the models described in the text.

**Scheme 2**

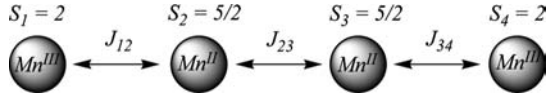


In order to avoid overparametrization, the magnetic anisotropy and especially the effects of axial zero-field splitting have been ignored in our first approach to model the obtained results.[45] Therefore, the isotropic Heisenberg spin Hamiltonian that describes this complex is given by eq 1:

$$H = -2J_{12}S_1 \cdot S_2 - 2J_{23}S_2 \cdot S_3 - 2J_{34}S_3 \cdot S_4 \qquad (1)$$

where $J_{12}$, $J_{23}$, and $J_{34}$ are the exchange interactions between Mn sites, as shown in Scheme 2, and $S_i$ represents the spin vectors for each metal ions ($S_i = 2$ for $Mn^{III}$ with $i = 1$ and 4 and $S_i = 5/2$ for $Mn^{II}$ with $i = 2$ and 3). The centrosymmetric linear topology of **1** imposes equality between $J_{12}$ and $J_{34}$ (called in the following $J_{wb}$, while $J_{23}$ will be noted $J_{bb}$). Therefore, eq 1 simplifies to a simple two-$J$ model, as displayed in eq 2:

$$H = -2J_{wb}(S_1 \cdot S_2 + S_3 \cdot S_4) - 2J_{bb}S_2 \cdot S_3 \qquad (2)$$

Since the Kambe/van Vleck method[46,47] is not applicable for the spin topology of **1**, a numerical approach[48,49] has been used to simulate the experimental data as shown by the red solid line in Figure 5. The best set of parameters obtained includes $J_{wb}/k_B = +4.0(1)$ K (2.8(1) $cm^{-1}$), $J_{bb}/k_B = +0.13(2)$ K (0.09(2) $cm^{-1}$), and $g_{av} = 1.96$, implying that this $Mn_4$ unit possesses an $S_T = 9$ spin ground state. It is worth noting that the above model reproduces extremely well the experimental data, and therefore it is impossible to add further parameters (such as single-ion magnetic anisotropy induced by the presence of $Mn^{III}$ metal ions or intermolecular magnetic interactions) without overparametrization. Nevertheless, it is important to mention that the value of $J_{bb}$ is certainly underestimated by the present approach due to the effects of magnetic anisotropy or intermolecular magnetic interactions that both would artificially reduce the obtained value.

The magnetic properties of several tetranuclear Mn complexes involving $Mn^{III}_2Mn^{II}_2$ valence combination have been summarized in Table 5. Most of these complexes have been prepared by self-assembly, in which the metal centers are connected by bridging oxo ($O^{2-}$), alkoxo ($OR^-$), or carboxylate ($RCOO^-$) groups, thus forming linear, bent, or even cubane-type moieties. $Mn^{II}$ ions in all of these compounds occupy the terminal or wingtip positions, while the central or body positions are taken up by the $Mn^{III}$ centers (see Table 5). The exchange interactions between these metal centers display a large range of values from antiferromagnetic[15b,17,45,50] ($J_{Mn(III)-Mn(II)} = J_{wb} = -1.5$ to $-41.7$ $cm^{-1}$ and $J_{Mn(II)-Mn(II)} = J_{bb} = -2.8$ to $-45$ $cm^{-1}$) to ferromagnetic ($J_{Mn(III)-Mn(II)} = J_{wb} = 1.1-6.58$ $cm^{-1}$ and $J_{Mn(II)-Mn(II)} = J_{bb} = -0.26$ to 8.7 $cm^{-1}$) ones depending on the nature of the bringing groups.[20,51,52] Compound **1** has an interesting structural particularity in comparison to the previous systems considering that the $Mn^{III}$ ions occupying the terminal positions while the $Mn^{II}$ ions are now in the center of the complex. Indeed, this structural topology has also been reported by Khanra et al.[53] It is worth mentioning that tetranuclear compounds[15b,17,45,50] displaying antiferromagnetic couplings between Mn ions have a common structural feature involving $\mu$-oxo bridge(s) that provides a super exchange ($d_{z^2}-d_{z^2}$ or $d_{z^2}-d_{xz}$) pathway.[54,55] Most of the compounds that posses intramolecular ferromagnetic interactions and an $S_T = 9$ ground state[20,51,52] also display a uniaxial zero-field splitting parameter ($D < 0$) induced by the presence of anisotropic manganese(III) ions. These combined characteristics, high-spin ground state and uniaxial anisotropy, generate their single-molecule magnet (SMM) properties. Compound **1**, however, failed to function as a SMM in spite of its $S_T = 9$ ground state, probably due to the presence of (i) low-lying excited states with smaller spin values and also (ii) weak magnetic anisotropy of the complex. This latter hypothesis is supported by (i) the excellent simulation of the $\chi T$ versus $T$ data (Figure 5) with a Heisenberg model that does not include magnetic anisotropy and (ii) the absence of a low-temperature decrease of the experimental $\chi T$ product that is usually seen (even at 1000 Oe) in the presence of a significant magnetic anisotropy.

For complex **2**, the value of the $\chi T$ product remains almost constant at ca. 10 $cm^3$ K $mol^{-1}$ between 300 and 40 K and then decreases to ca. 5.9 $cm^3$ K $mol^{-1}$ at 1.8 K. The susceptibility at room temperature is close to the spin-only value (10.03 $cm^3$ K $mol^{-1}$) expected for one $S = 5/2$ $Mn^{II}$ and two $S = 2$ $Mn^{III}$ ions in the high-temperature Curie limit. The drop in the $\chi T$ product below 10 K suggests the presence of magnetic anisotropy expected for $Mn^{III}$ ions, inter- or more likely intramolecular antiferromagnetic couplings. Therefore, as a first approach, this magnetic behavior has been analyzed taking into account only isotropic neighboring magnetic interactions within the trinuclear complex. Application of the van Vleck equation[47] to Kambe's vector coupling scheme[46] allows us to determine the analytical low-field limit

(45) Thorp, H. H.; Sarneski, J. E.; Kulawiec, R. J.; Brudvig, G. W.; Crabtree, R. H.; Papaefthymiou, G. C. *Inorg. Chem.* **1991**, *30*, 1153.
(46) Kambe, K. *J. Phys. Soc. Jpn.* **1950**, *5*, 48.
(47) van Vleck, J. H. *The Theory of Electric and Magnetic Susceptibility*; Oxford University Press: Oxford, 1932.
(48) Borras-Almenar, J. J.; Clemente-Juan, J. M.; Coronado, E.; Tsukerblat, B. S. *Inorg. Chem.* **1999**, *38*, 6081.
(49) Borras-Almenar, J. J.; Clemente-Juan, J. M.; Coronado, E.; Tsukerblat, B. S. *J. Comput. Chem.* **2001**, *22*, 985.
(50) Vincent, J. B.; Christmas, C.; Chang, H.-R.; Li, Q.; Boyd, P. D. W.; Huffman, J. C.; Hendrickson, D. N.; Christou, G. *J. Am. Chem. Soc.* **1989**, *111*, 2086.
(51) Wittick, L. M.; Murray, K. S.; Moubaraki, B.; Batten, S. R.; Spiccia, L.; Berry, K. J. *J. Chem. Soc., Dalton Trans.* **2004**, 1003.
(52) Yoo, J.; Brechin, E. K.; Yamaguchi, A.; Nakano, M.; Huffman, J. C.; Maniero, A. L.; Brunel, L.-C.; Awaga, K.; Ishimoto, H.; Christou, G.; Hendrickson, D. N. *Inorg. Chem.* **2000**, *39*, 3615.
(53) Khanra, S.; Weyhermuller, T.; Bill, E.; Chaudhuri, P. *Inorg. Chem.* **2006**, *45*, 5911.
(54) Bossek, U.; Weyhermuller, T.; Weighardt, K.; Bonvoisin, J.; Girerd, J. J. *J. Chem. Soc., Chem. Commun.* **1989**, 633.
(55) Sheats, J. E.; Czernuszewicz, R. S.; Dismukes, G. C.; Rheingold, A. L.; Petrouleas, V.; Stubbe, J.; Armstrong, W. H.; Beer, R. H.; Lippard, S. J. *J. Am. Chem. Soc.* **1987**, *109*, 1435.

**Table 5.** Magnetic and Structural Parameters for the Tetranuclear $Mn^{III}_2Mn^{II}_2$ Complexes

| complex/structural type[a] | $J_{wb}$, $cm^{-1}$ | $J_{bb}$, $cm^{-1}$ | $g$ | ref |
|---|---|---|---|---|
| $[Mn_4(tpdp)_2(CH_3COO)_2(\mu\text{-}O)(H_2O)_2](CF_3SO_3)_4\cdot 2H_2O$/ $Mn^{II}-Mn^{III}-Mn^{III}-Mn^{II}$, linear | −6 | −45 | 2.0 | 15b |
| $[Mn_4(tqhpn)_2(\mu\text{-}O)_2(H_2O)_2](ClO_4)_4\cdot 6CH_3CN\cdot 2Et_2O$/ $Mn^{II}-Mn^{III}-Mn^{III}-Mn^{II}$, linear | −41.7 | −2.8 | 1.95 | 17 |
| $[Mn_4(\mu_3\text{-}O)_2(O_2CCPh_3)_6(OEt_2)]/Mn^{II}-Mn^{III}-Mn^{III}-Mn^{II}$, nonlinear | −1.5 | −2.8 | 1.47 | 45 |
| $[Mn_4(\mu_3\text{-}O)_2(CH_3COO)_6(bipy)_2]\cdot 2CHCl_3/Mn^{II}-Mn^{III}-Mn^{III}-Mn^{II}$, nonlinear | −1.97 | −3.12 | 1.70 | 50 |
| $[Mn_4(6\text{-}Mehmp)_6Cl_4]\cdot 4H_2O/Mn^{II}-Mn^{III}-Mn^{III}-Mn^{II}$, bent-linear | 6.58 | −0.26 | 1.96 | 19a |
| $[Mn_4(L^3H_2)_2(L^3H)_2(H_2O)_2(MeCOO)_2](MeCOO)_2 2H_2O$/ $Mn^{II}-Mn^{III}-Mn^{III}-Mn^{II}$, nonlinear | 1.7 | 6.5 | 1.89 | 51 |
| $[Mn_4(CH_3COO)_2(pdmH)_6](ClO_4)_2\cdot 2.5H_2O/Mn^{II}-Mn^{III}-Mn^{III}-Mn^{II}$, nonlinear | 1.1 | 8.7 | 1.89 | 52 |
| $[Mn_4(L^1)_2(PhCOO)_6]/Mn^{III}-Mn^{II}-Mn^{II}-Mn^{III}$, linear | 2.76 | 0.089 | 1.96 | this work |
| $[L_2Mn^{III}_2\{\mu\text{-}(dfmp)_3Mn^{II}_2\}]ClO_4/Mn^{III}-Mn^{II}-Mn^{II}-Mn^{III}$, linear | 2.4 | −9.1 | 1.9 | 53 |

[a] Htpdp = N,N,N′,N′-tetrakis(2-pyridylmethyl)-1,3-diamino-2-propanol; Htqhpn = N,N,N′,N′-tetrakis(2-quinolylmethyl)-2-hydroxy-1,3-propanediamine; 6-Mehmp = 6-methyl-2-hydroxymethylpyridine; $L^3H_3$ = triethanolamine; $pdmH_2$ = pyridine-2,6-dimethanol; L = 1,4,7-trimethyl-1,4,7,-triazacyclononane; $H_3$dfmp = 2,6-diformyl-4-methylphenol oxime.

expression[56] of magnetic susceptibility from the following spin Hamiltonian:

$$H = -2J_{12}S_1\cdot S_2 - 2J_{23}S_2\cdot S_3 \quad (3)$$

where $S_i$ is the spin and $J_{12}$ and $J_{23}$ are the intramolecular exchange interactions between Mn sites and vectors for each metal ion ($S_i = 2$ for $Mn^{III}$ with $i = 1$ and 3 and $S_2 = 5/2$ for $Mn^{II}$). Even if the molecular structure of **2** is not strictly centrosymmetrical, the geometrical similarity between the two $Mn^{III}-Mn^{II}$ bridges suggests consideration of the two intramolecular interactions as identical in our model ($J_{12} = J_{23} = J$). A good least-squares fit has been achieved (solid line, Figure 5) with $J/k_B = -0.19(1)$ K ($0.13(1)$ $cm^{-1}$) and $g_{av} = 1.96$. The antiferromagnetic nature of the interaction between $Mn^{II}$ and $Mn^{III}$ stabilizes an $S_T = 3/2$ spin ground state for this complex. The observed magnetic behavior is consistent with the relatively weak antiferromagnetic interactions observed between $Mn^{II}$ and $Mn^{III}$ ions, in several $Mn^{II}Mn^{III}$ binuclear complexes.[57−59] Analoguous trinuclear $Mn^{III}-Mn^{II}-Mn^{III}$ complexes have also been reported,[23,24,29,42,43,60] with different combinations of carboxylate, phenolate, hydroxo, or alkoxo bridging moieties that favor either antiferromagnetic[23,24,42,43] or ferromagnetic exchange,[29] depending upon the type of the bridging ligands that control the super exchange pathway(s).[24] Nevertheless, in all of these compounds, like in **2**, the super exchange interaction is always weak ($J$ range between −7 to +3 $cm^{-1}$).

The X-band EPR spectrum of compound **1** in a $CH_2Cl_2$/toluene (1:10 v/v) solution at room temperature displayed a broad feature in the $g \approx 2$ region (Figure S1, Supporting Information). Similar broad features appear to be characteristic of tetranuclear $Mn^{III}_2Mn^{II}_2$ complexes, as reported earlier.[17,45] In frozen solution (12 K), however, the spectrum also contains an additional six-line ($^{55}Mn$, $I = 5/2$) feature ($A = 8.8$ mT) at $g \approx 4$ region (Figure 6). Hyperfine lines are also observable with the $g \approx 2$ signal at this extreme low temperature. Results indicate medium to weak interactions among the manganese centers in compound **1**, as revealed from the susceptibility measurements. Compound **2** is EPR-inactive.

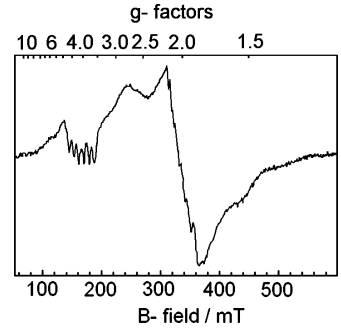


**Figure 6.** X-band EPR spectrum of compound **1** in a frozen $CH_2Cl_2$/toluene (1:10 v/v) solution at 12 K.

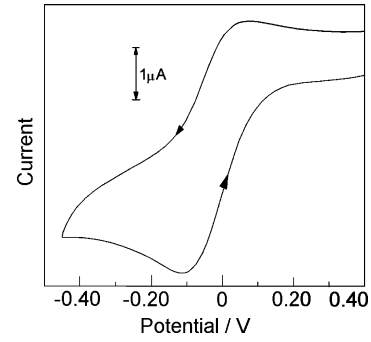


**Figure 7.** Cyclic voltammogram of **1** in $CH_2Cl_2$ solution (containing 0.1 M TBAP) at a platinum disk working electrode (scan rate 100 mV $s^{-1}$ and potential recorded vs Ag/AgCl).

**Cyclic Voltammetry.** The redox behaviors of **1** and **3** have been examined by cyclic voltammetry at a platinum disk working electrode under an envelope of purified dinitrogen. Compound **1** displays a reduction process at $E_{1/2} = -0.03$ V versus a Ag/AgCl reference in dichloromethane solution (Figure 7) which may be labeled as quasireversible ($\Delta E_p = 165$ mV) in the electrochemical sense.[61] Unfortunately, the reduced species is not sufficiently stable for the coulometric evaluation of the number of electrons involved in the process.

(56) Vincent, J. B.; Chang, H.-R.; Folting, K.; Huffman, J. C.; Christou, G.; Hendrickson, D. N. *J. Am. Chem. Soc.* **1987**, *109*, 5703.
(57) Buchanan, R. M.; Oberhausen, K. J.; Richardson, J. F. *Inorg. Chem.* **1988**, *27*, 971.
(58) Diril, H.; Chang, H.-R.; Zhang, X.; Larsen, S. K.; Potenza, J. A.; Pierpont, C. G.; Schugar, H. J.; Isied, S. S.; Hendrickson, D. N. *J. Am. Chem. Soc.* **1987**, *109*, 6207.
(59) Chang, H.-R.; Larson, S. K.; Boyd, P. D. W.; Pierpont, C. G.; Hendrickson, D. N. *J. Am. Chem. Soc.* **1988**, *110*, 4565.
(60) Kitajima, N.; Osawa, M.; Imai, S.; Fujisawa, K.; Moro-oka, Y.; Heerwegh, K.; Reed, C. A. *Inorg. Chem.* **1994**, *33*, 4613.

The voltammogram of **3** in methanol also involves a sole reduction process at $E_{pc} = 0.24$ V. The reduced species is not stable enough to appear in the reverse scan of 200 mV $s^{-1}$. At a higher scan rate ($v > 400$ mV $s^{-1}$), however, the species does survive to appear as a quasireversible voltammogram at $E_{1/2} = -0.11$ V ($\Delta E_p = 256$ mV), as displayed in Figure S2 (in the Supporting Information). We believe this process is due to a metal-centered one-electron $Mn^{III}/Mn^{II}$ transfer, which we failed to prove conclusively due to the instability of this compound on the longer time scale of coulometry. Compound **2** is however electrode-inactive.

## Concluding Remarks

Sterically constrained tetradentate ligand $H_2L$ has been used to synthesize mono-, tri-, and tetranuclear manganese(II/III) complexes in the presence of ancillary carboxylate ligands, providing varied steric congestions and electronic influences that ultimately control the nuclearity of the final products. With a benzoate ligand, the product $[Mn_4(L)_2(PhCOO)_6]$, **1**, is a mixed-valence $Mn^{III}_2Mn^{II}_2$ tetranuclear compound with an interesting molecular structure in the form of a "dimer-of-dimers" model in relation to the water oxidation apparatus, available in photosystem-II.[4,5] Compound **1** displays intramolecular ferromagnetic interactions that stabilize an $S_T = 9$ ground state but fails to exhibit single-molecule magnet behavior due to the presence of low-lying excited states with smaller spin values and a weak magnetic anisotropy. While with a propionate ligand, the product is a mixed-valence trinuclear compound $[Mn_3(L)_2(CH_3CH_2COO)_2(OMe)_2]\cdot H_2O$, **2**, with an $S_T = 3/2$ spin ground state, the bulky pivalate on the other hand induces a mononuclear manganese(III) compound $[Mn(L)\{(CH_3)_3CCOO\}(CH_3OH)]\cdot CH_3OH$, **3**. This compound has a unique molecular structure containing a monodentate pivalate group that restricts the molecule to have a mononuclear status due to the steric and electronic influences imposed by the *tert*-butyl group of the pivalate anion. The monodentate carboxylate here is stabilized by strong hydrogen bonding from an axially coordinated methanol molecule that completes the octahedral geometry around $Mn^{III}$ along with the $N_2O_2$ donors of the capping $L^{2-}$ ligand.

**Acknowledgment.** Financial support received from the Council of Scientific and Industrial Research (CSIR), New Delhi, is gratefully acknowledged. Three of us (D.M., P.B.C., and S.B.) also thank the CSIR for the award of Research Fellowships. Crystallography was done in part at the DST-sponsored National Single Crystal X-ray Diffraction Facility at IACS. We also thank Professor K. Nag and Dr. Meenakshi Ghosh for their help in electrochemical and EPR experiments, respectively. R.C. thanks the Bordeaux 1 University, the CNRS, and the "Région Aquitaine" for financial support.

**Supporting Information Available:** Room-temperature EPR spectrum of **1** in solution (Figure S1), the cyclic voltammogram of **3** in methanol (Figure S2), and X-ray crystallographic files in CIF format for compounds **1**−**3**. This material is available free of charge via the Internet at http://pubs.acs.org.

IC801132R

(61) Brown, E. R.; Large, R. F. Electrochemical Methods. In *Physical Methods in Chemistry*; Weissberger, A., Rossiter, B., Eds.; Wiley-Interscience: New York; Part IIA, Chapter VI, p 1071.